

Anomalous relaxation and multiple timescales in the quantum XY model with boundary dissipationShun-Yao Zhang,¹ Ming Gong,^{1,2,3,*} Guang-Can Guo,^{1,2,3} and Zheng-Wei Zhou^{1,2,3,†}¹*CAS Key Laboratory of Quantum Information, University of Science and Technology of China, Hefei 230026, People's Republic of China*²*Synergetic Innovation Center of Quantum Information and Quantum Physics, University of Science and Technology of China, Hefei, Anhui 230026, China*³*CAS Center For Excellence in Quantum Information and Quantum Physics, University of Science and Technology of China, Hefei, Anhui, 230026, China*

(Received 26 March 2019; revised manuscript received 29 March 2020; accepted 31 March 2020; published 30 April 2020)

The relaxation of a many-body system is still a challenging problem that has not been well understood. In this work we exactly calculate the dynamics of the quantum XY model with boundary dissipation, in which the density matrix in terms of Majorana operators can be decoupled into independent subspaces \mathcal{K}_i represented by different number of Majorana fermions. The relaxation is characterized by multiple timescales, and in the long-time limit it is determined by the single-particle relaxation process in a typical timescale T^* . For the bulk bands, we find $T^* \propto N^3/\gamma n^2$ in the weak dissipation limit and $T^* \propto \gamma N^3/n^2$ in the strong dissipation limit, where N is the chain length, γ is the dissipation rate, and n is the band index. For the edge modes, $T^* \propto 1/\gamma$ indicates the most vulnerable to dissipation in the long-chain limit. These results are counterintuitive because it means any weak dissipation can induce strong relaxation, while strong dissipation can induce weak relaxation. We find that these two limits correspond to two different physics, which are explained based on the first- and second-order perturbation theory in an equivalent non-Hermitian model. Finally, we show that even in the long-chain limit with weak dissipation, the relaxation may exhibit strong odd-even effect, which can be washed out by the strong dissipation. These results shed new insight into the dynamics of topological qubits in the environment, and the mechanism for many-body dissipation may also have universal significance in understanding the many-body dissipation in the other models.

DOI: [10.1103/PhysRevB.101.155150](https://doi.org/10.1103/PhysRevB.101.155150)**I. INTRODUCTION**

The isolated quantum system can be well described by the time-dependent Schrödinger equation. However, the quantum systems are inevitable to interact with the environment, which can lead to various dissipation behaviors. While the dynamics of qubits in the environment have been well studied [1,2], the same issue in the many-body systems is still one major challenge in theory [3–15] due to the more expensive computation cost [16] and the more complicated dissipation channels involved. However, this is an important question at least from two diverse aspects. First, the many-body systems may possess some features that are totally different from the single-particle systems, such as ergodicity and thermalization [17,18], which are fundamental concepts in statistical physics. In the trapped ions, it may exhibit different dynamics depending strongly on the initial states, which are explained based on quantum many-body scar [19–21]. Second, it is also an important issue in topological quantum computation [22–24], in which the two ground states are separated from the excited bands by a finite energy gap [25–33]. Thus, if the temperature is much lower than the excitation gap, then the occupation of the excited states is exponentially small and thus is negligible. This picture is not necessarily true in the

presence of dissipation, which can induce direct coupling between ground states and excited states. A possible mechanism to go beyond the stability of topological protected modes in terms of quasiparticle poisoning has been discussed [34,35].

Here we explore the roles of edge modes and bulk bands in the dynamics of the quantum XY model with boundary dissipation. We consider this model for several basic reasons. First, when the system is interacting with the other controlled systems, the dissipation is more likely to be introduced to the system from the two contacted regimes. Second, this model can be solved analytically in several limits, thus the dissipation of the many-body states in terms of many-body and single-particle dissipation can be seen easily. Third, this model, after a proper transformation, can be mapped to the p -wave superconducting model [36], which can be used for the realization of Majorana zero modes at the two open ends for topological quantum computation. The major findings in this work can be summarized as follows:

(i) In terms of Majorana operators, the density matrix is decoupled into different subspaces represented by different number of Majorana fermions. In time evolution, the density matrix exhibits multiple relaxation scales, in which the slowest decay is given by the single-particle relaxation with longest relaxation process. This timescale T^* is used to determine the relaxation time of the many-body ground state with dissipation.

*gongm@ustc.edu.cn

†zwwzhou@ustc.edu.cn

(ii) In the weak dissipation limit, $T^* \propto N^3/\gamma$, where N is the total chain length and γ is the boundary dissipation rate. However, in the strong dissipation limit, $T^* \propto \gamma N^3$. The edge modes are shown to be most vulnerable to dissipation due to $T^* \propto 1/\gamma$. These results are counterintuitive because it means that weak dissipation can induce fast relaxation, while strong dissipation can induce weak relaxation. We understand these results by mapping the single-particle dynamics to a non-Hermitian model and derive the analytical results using perturbation theory with a proper decomposition of the non-Hermitian Hamiltonian.

(iii) These dynamics exhibits strong odd-even effect in the weak dissipation limit. However, in the strong dissipation limit, which greatly influences the single-particle behavior, the odd-even effect is washed out. These results shed new insight into the dissipation and relaxation of the topological qubits in the environment.

These results yield a new picture for the understanding of the many-body dissipation in terms of single-particle and many-body dissipation. In the short-time regime, the many-body dissipation is dominated; however, in the long-time limit, which is used to characterize the relaxation time T^* , it is determined by the single-particle dissipation. This manuscript will be organized as follows. In Sec. II, we will discuss the quantum XY model subjected to boundary dissipation and the related representation of the density matrix using Majorana fermions. In Sec. III, we will discuss the evolution of the density matrix and its multiple timescales. In Sec. IV, the approximated solutions of the eigenvalues in the weak dissipation limit and strong dissipation limit are discussed. The mechanisms for these results based on perturbation theory, in which the above two limits will have totally different physics, will be presented in Sec. V. Finally, we conclude in Sec. VI. More details about the derivation of these results will be presented in Appendices A–D.

II. MODEL AND MASTER EQUATION

We consider a quantum XY model with boundary dissipation, whose Lindblad equation in terms of the density matrix ρ reads as

$$\dot{\rho} = \mathcal{L}(\rho) = -i[H_{XY}, \rho] + \mathcal{D}(\rho). \quad (1)$$

Here the Hamiltonian of the XY model [37–41] and its boundary dissipation by the Lindblad operator [42,43] can be written as

$$H_{XY} = - \sum_{i=1}^{N-1} (g_1 \sigma_i^x \sigma_{i+1}^x + g_2 \sigma_i^y \sigma_{i+1}^y), \quad (2)$$

$$\mathcal{D}(\rho) = \frac{\gamma}{2} \sum_{j=1, N} (2\sigma_j^z \rho \sigma_j^z - 2\rho), \quad (3)$$

where γ is termed as the dissipation rate and N is the total chain length. Here we assume $g_1 > g_2 > 0$, while the other conditions can be connected to this case through some unitary transformations (see the symmetry transformations for the quantum XY model in Appendix A). This model can be fermionized to a p -wave superconducting model using Majorana operators via the Jordan-Wigner transformation as

follows:

$$\alpha_{2j-1} = \left(\prod_k^{j-1} \sigma_k^z \right) \sigma_j^x, \quad \alpha_{2j} = \left(\prod_k^{j-1} \sigma_k^z \right) \sigma_j^y, \quad (4)$$

where α_i are Majorana fermions satisfying $\{\alpha_i, \alpha_j\} = 2\delta_{ij}$. With this, we have [36,44,45]

$$H_{XY} = ig_1 \sum_{j=1}^{N-1} \alpha_{2j} \alpha_{2j+1} - ig_2 \sum_{j=1}^{N-1} \alpha_{2j-1} \alpha_{2j+2}. \quad (5)$$

Notice that throughout this work, the subscript in the XY model has been removed when the model is transferred to the fermion representation. In this case, the Lindblad operator is still made by local dissipation as follows:

$$\mathcal{D}(\rho) = -\gamma \sum_{j=1, N} (\alpha_{2j-1} \alpha_{2j} \rho \alpha_{2j-1} \alpha_{2j} + \rho). \quad (6)$$

This operator can also be rewritten in terms of canonical fermions as

$$\mathcal{D}(\rho) = \gamma \sum_{j=1, N} (4c_j^\dagger c_j \rho c_j^\dagger c_j - 2c_j^\dagger c_j \rho - 2\rho c_j^\dagger c_j), \quad (7)$$

where $c_1 = (\alpha_1 + i\alpha_2)/2$ and $c_N = (\alpha_{2N-1} + i\alpha_{2N})/2$. The similar feature can be found when the dissipation is located at the other sites.

First, let us consider the case with $\gamma = 0$. Then the spectra between the XY model and p -wave superconducting model are related by

$$E = \sum_i n_i \epsilon_i, \quad n_i = \{0, 1\}, \quad (8)$$

where ϵ_i are single-particle spectra in p -wave superconducting model and E is the many-body spectra in XY model. Thus, the N eigenvalues from the single particle Hamiltonian can be used to construct all the 2^N eigenvalues in the quantum XY model [see Figs. 1(a) and 1(c)]. In the fermion representation, the two localized zero modes at the open ends give rise to the twofold degeneracy in the XY model. We focus on $g_1 > 0$ and $g_2 > 0$, and the phase diagram for the XY model and its corresponding single fermion phases are given in Fig. 1(b), with boundary at $\lambda = g_2/g_1 = 1$ (see Appendix A). In fermion representation, it can be regarded as two separate Majorana chains $A(\alpha_1, \alpha_4, \alpha_5, \dots)$ and $B(\alpha_2, \alpha_3, \alpha_6, \dots)$, as shown in Fig. 1(d). We can bring Eq. (5) to a form of paired Majorana operators [36,46],

$$H = \frac{i}{2} \sum_{k=1}^{N-1} \epsilon_k b'_k b''_k + \frac{i\delta E_c}{2} \alpha_L \alpha_R, \quad (9)$$

where $\delta E_c \sim e^{-N/\xi} [(-1)^N + 1]$. After a special orthogonal transformation, the Hamiltonian in Eq. (9) can be brought into small Jordan blocks, with b'_k and b''_k being some new Majorana operators, following the pioneering work by Kitaev [36]. By a transformation from Majorana fermion to canonical fermion,

$$c_k = (b'_k + ib''_k)/2, \quad c_k^\dagger = (b'_k - ib''_k)/2, \quad (10)$$

the spectra of the bulk bands can be obtained as $\pm\epsilon_k$. In the last term, α_L and α_R are edge modes at the left and right edges, which can be written as $\alpha_L = \alpha_1 - \lambda\alpha_5 + \lambda^2\alpha_9 - \dots$ and α_R

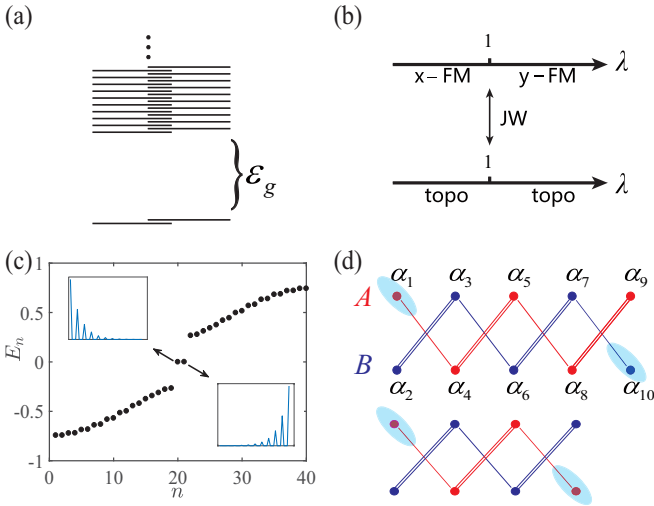


FIG. 1. (a) The two lowest energy levels in the XY model are separated from the excited bands by an energy gap ϵ_g . (b) Phase diagram. The two ferromagnetic (FM) phases in the XY model will be mapped to two distinct topological p -wave superconducting phases after fermionization. The phase boundary given by $g_1 = g_2$ is shown in Appendix A. (c) Energy levels in the fermion representation, in which the two edge modes, occupied or unoccupied, give the twofold degeneracy of the XY model. (d) The odd-even effect due to the oscillation of coupling between the two edge modes in the two subchains A and B with weak dissipation.

$= \alpha_{2N} - \lambda \alpha_{2N-4} + \lambda^2 \alpha_{2N-8} - \dots$ (for $\lambda < 1$). In δE_c , $\xi \propto 1/|\ln g_1 - \ln g_2|$ defines the correlation length [36]. This odd-even effect is a typical feature of coupling between two distant zero modes, which may happen even in the continuous space [47]. With these operators, the two ground states in Fig. 1(a) can be written as

$$|1\rangle = \frac{1 + \alpha_L}{\sqrt{2}} |0\rangle, \quad |2\rangle = \frac{1 - \alpha_L}{\sqrt{2}} |0\rangle, \quad (11)$$

where $|0\rangle = \prod_k c_k^\dagger |\text{vac}\rangle$ is the state that all levels with energy smaller than zero are occupied. This is the ground state of the many-body XY model. In the thermodynamic limit, the above two states are energetically degenerate.

When γ is switched on, the many-body dynamics will respect the parity symmetry $[\mathcal{L}, P] = 0$, with

$$P = \prod_j^N \sigma_j^z = i^N \prod_j^{2N} \alpha_j. \quad (12)$$

This parity operator satisfies $P^2 = 1$. This parameter operator in the second equal mark was used by Kitaev in the derivation of the edge modes in the one dimensional spinless model in proximity with a p -wave superconductor [36]. This parity operator accounts for the twofold ground-state degeneracy of the zero modes. Since it is a product of all σ_j^z operators or all the Majorana fermion operators, it is robust against local perturbation. In the long-time limit when approaching the steady solution, only this symmetry operator is important and we have

$$\bar{\rho} = \lim_{t \rightarrow \infty} \rho(t) = (I + wP)/2^N, \quad (13)$$

where $w = \langle \Psi_0 | P | \Psi_0 \rangle$ is determined by the initial wave function. This corresponds to the maximally mixed state at infinite high temperature.

III. EVOLUTION OF THE DENSITY MATRIX

A. Majorana fermion representation

In general, there are two different ways to express the density matrix. In the spin representation, it can be expressed as

$$\rho_{XY} = \frac{1}{2^N} \sum_{o_i=\{0,1,2,3\}} \rho_{\sigma} \sigma_1^{o_1} \otimes \sigma_2^{o_2} \otimes \sigma_3^{o_3} \cdots \otimes \sigma_N^{o_N}, \quad (14)$$

where we have defined $\sigma^0, \sigma^1, \sigma^2, \sigma^3$ to be Pauli matrix $1, \sigma^x, \sigma^y, \sigma^z$ and $\sigma = (\sigma_1^{o_1}, \sigma_2^{o_2}, \sigma_3^{o_3}, \dots, \sigma_N^{o_N})$. The coefficient ρ_{σ} can be obtained from

$$\rho_{\sigma} = \text{Tr}(\rho_{XY} \sigma_1^{o_1} \otimes \sigma_2^{o_2} \otimes \sigma_3^{o_3} \cdots \otimes \sigma_N^{o_N}). \quad (15)$$

This density matrix has the dimension of $2^N \times 2^N$, and the total possibility of basis is 4^N , which is too complex to be solved analytically. A novel way is to express the total Hamiltonian in terms of Majorana operators as follows [48–50]:

$$\rho = \frac{1}{2^N} \sum c_{a_1, a_2, \dots, a_{2N}} \alpha_1^{a_1} \alpha_2^{a_2} \cdots \alpha_{2N}^{a_{2N}}, \quad (16)$$

where $a_j = \{0, 1\}$. Notice that the total number of basis in this new representation is also 4^N , which is exactly the same as that in the spin representation ρ_{XY} . In principle, there is a one-to-one correspondence between these two representations (see several examples in Appendix B), thus they are equivalent.

B. Multiple timescales

We can prove that the master equation preserves the number of Majorana operators (see details in Appendix C), which is given by $n = \sum_i a_i$, thus the dynamics of ρ is decoupled into different subspaces denoted as \mathcal{K}_n for $n = 0 - 2N$. For this reason, we can define

$$\mathcal{K} = \mathcal{K}_0 \oplus \mathcal{K}_1 \oplus \mathcal{K}_2 \oplus \cdots \oplus \mathcal{K}_{2N}, \quad (17)$$

where the dimension of \mathcal{K}_i is C_{2N}^i . We can readily check that the dimension of \mathcal{K} (the whole dimension of the Hamiltonian) is $C_{2N}^0 + C_{2N}^1 + C_{2N}^2 + \cdots + C_{2N}^{2N} = 4^N$. This decoupling is essentially the same as the probability distribution in the classical Ising model by Glauber [51]. By a direct comparison with Eq. (13), we can find that while the first term ($a_j \equiv 0$) and the last term ($a_j \equiv 1$) are unchanged, which gives Eq. (13), all the other terms will disappear in the long-time limit.

In principle, the dynamics of ρ can be calculated using the hierarchy equations, similar to that used in Ref. [51]. In general, the dynamics in all the subspaces \mathcal{K}_i are coupled. To this end, we may define the following variables:

$$\begin{aligned} \psi_i &= \text{Tr}(\rho \alpha_i), \\ \psi_{ij} &= \text{Tr}(\rho \alpha_i \alpha_j), \\ \psi_{ijk} &= \text{Tr}(\rho \alpha_i \alpha_j \alpha_k), \end{aligned} \quad (18)$$

with $i \neq j \neq k$ and then calculate their time evolution based on the Heisenberg equations (see details in Appendix C). We

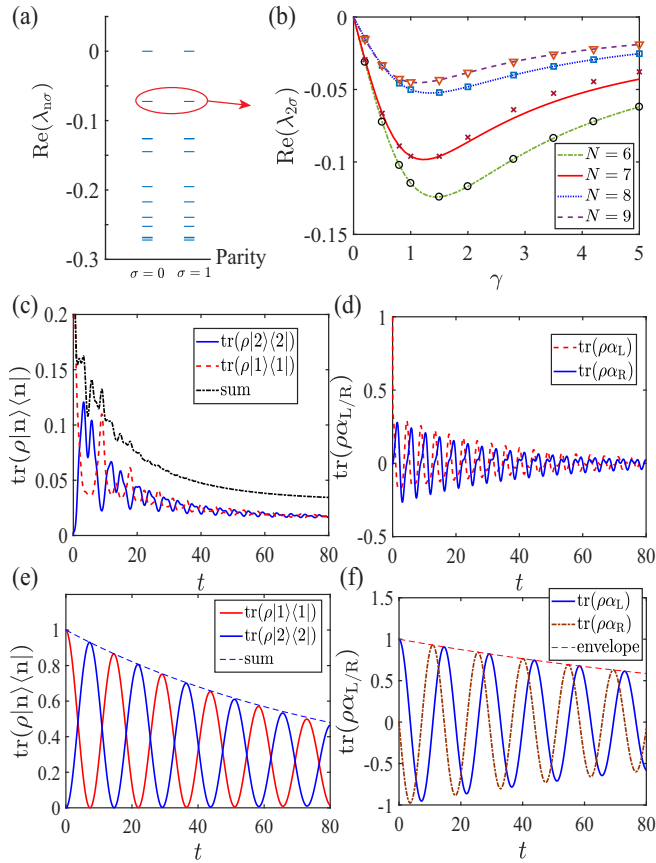


FIG. 2. (a) Eigenvalues $\text{Re}(\lambda_{n\sigma})$ of the super-operator \mathcal{L} in XY model with $N = 6$, $\gamma = 0.5$. Here $\text{Re}(\lambda_{n\sigma})$ is arranged in descending order with $\text{Re}(\lambda_{n\sigma}) \geq \text{Re}(\lambda_{n+1\sigma})$, and $\sigma = 0, 1$ accounts for different parity. (b) The lines are eigenvalues of $H_0 + i\Gamma$ [see Eq. (21)] with smallest imaginary energy and symbols are $\text{Re}(\lambda_{2\sigma})$ of \mathcal{L} . In both figures $g_1 = 1.0$, $g_2 = 0.7$. Panels (c) and (d) show the projection of $\rho(t)$ to the ground state of the XY model $|n\rangle$ ($n = 1, 2$); and to the edge modes $\alpha_{R/L}$ of the fermion model, respectively, where $\rho(0) = |1\rangle\langle 1|$. In both figures $g_1 = 1.0$, $g_2 = 0.7$, $N = 6$, and $\gamma = 20$. Panels (e) and (f) plot the same results as panels (c) and (d) with dissipation rate $\gamma = 0.005$.

find that for the boundary dissipation in Eq. (1), the dynamics of these variables are restricted to their own subspaces $\mathcal{K}_{1,2,3}$ due to the reason proved in details in Eq. (C5). This limit will show up the multiple timescales during dynamics much more clearly. Obviously, this approach can be generalized to models with more complicated dissipation and many-body interaction.

We first compare the full calculation of ρ against the dynamics in subspace \mathcal{K}_1 . In Fig. 2(a), we present the real part of the eigenvalues of superoperator \mathcal{L} of Eq. (1), in which the two zero eigenvalues correspond to the unchanged state in \mathcal{K}_0 and \mathcal{K}_{2N} subspaces. We also calculate the corresponding eigenvalues of this superoperator in the subspace constructed by \mathcal{K}_1 , which is given in Fig. 2(b). We find that the smallest eigenvalue $\text{Re}(\lambda_{1\sigma})$ of the \mathcal{L} in the XY model is the same as the spectra in \mathcal{K}_1 subspace, indicating that in the long-time limit, all the higher-order terms in $\mathcal{K}_{k \geq 2}$ subspaces decay much faster than that in \mathcal{K}_1 , leaving \mathcal{K}_1 to be dominated

relaxation channel for the quantum XY model. In Fig. 2(b), we find that while the increasing of the decay rate is observed with the increasing of dissipation rate in the weak dissipation limit, it is greatly suppressed in the strong dissipation limit, with an inflexion point happens near $\gamma \sim 1$. In Figs. 2(c) and 2(d), we show the projection of $\rho(t)$ to the ground states of the XY model and the edge modes. In Fig. 2(c), it will approach $1/2^N$ [$w = 0$ in Eq. (13)]; while in Fig. 2(d), it will approach zero, as expected.

To reinforce this conclusion, we also calculate the eigenvalues of the superoperator \mathcal{L} in subspaces \mathcal{K}_2 and \mathcal{K}_3 . Let us denote the eigenvalues as λ in each subspace. We find that, roughly, the slowest decay rate in \mathcal{K}_2 is two times faster than that in \mathcal{K}_1 . Similarly, the decay rate in \mathcal{K}_3 is much faster than that in \mathcal{K}_2 . Similar relations can be found in Ref. [51] by a finite truncation of the hierarchy equations. Thus, in the long-time and long-chain limits, we can fully characterize the relaxation time of the many-body system in terms of the single-particle and the few-particle dynamics. This observation may have universal significance, which may applicable to the other many-body systems.

With this density matrix, we can understand the dynamics in the many-body state for any given initial wave function. For example, for the results in Figs. 2(c) and 2(e), we can express the dynamics of $|n\rangle\langle n|$ as

$$\begin{aligned} \text{Tr}(\rho(t)|n\rangle\langle n|) &= \frac{1}{2^N} \left(c_{0\dots} + \sum_i c_{0\dots 1\dots 0}(t) \langle n|\alpha_i|n\rangle \right. \\ &\quad + \sum_{ij} c_{0\dots 1\dots 1\dots 0}(t) \langle n|\alpha_i\alpha_j|n\rangle \\ &\quad \left. + \sum_{ijk} c_{0\dots 1\dots 1\dots 1\dots 0}(t) \langle n|\alpha_i\alpha_j\alpha_k|n\rangle + \dots \right), \end{aligned} \quad (19)$$

where the coefficients can be determined by calculating the dynamics of the density matrix ρ in each subspace \mathcal{K}_i . Initially, we may find that the coefficients $c_{a_1, a_2, \dots, a_{2N}}$ and the overlap $\langle n|\alpha_1^{a_1}\alpha_2^{a_2}\dots\alpha_{2N}^{a_{2N}}|n\rangle$ are in the order of unity, which after a long-time relaxation will approach the steady solution as shown in Eq. (13). For this reason, not only the single-particle terms, but also all the many-particle terms, which correspond to the many-body relaxation, will contribute to the relaxation process. As a result, we find that the dynamics of the many-body state will exhibit multiple timescales during relaxation, in which some of these lifetimescales are shown in Fig. 3 (more details about the eigenvalues in the $\mathcal{K}_{1,2,3}$ subspaces in Fig. 3 are presented in Table I). We find that in the \mathcal{K}_2 and \mathcal{K}_3 subspaces, the eigenvalues of the superoperator \mathcal{L} in these spaces can be approximated (with high accuracy) as

$$\lambda_{i'}^2 = \lambda_i^1 + \lambda_j^1, \quad \lambda_{i'}^3 = \lambda_i^1 + \lambda_j^1 + \lambda_k^1, \quad (20)$$

where λ_i^k is the eigenvalues of the superoperator \mathcal{L} in \mathcal{K}_k subspace. The similar feature can be found even in the classical spin model [51]. Thus, due to the presence of these multi-particle relaxations, we find that in general the decay rates of many-particle states are faster than the single-particle ones (see Fig. 2 and data in Table I). Notice that in Figs. 2(e)

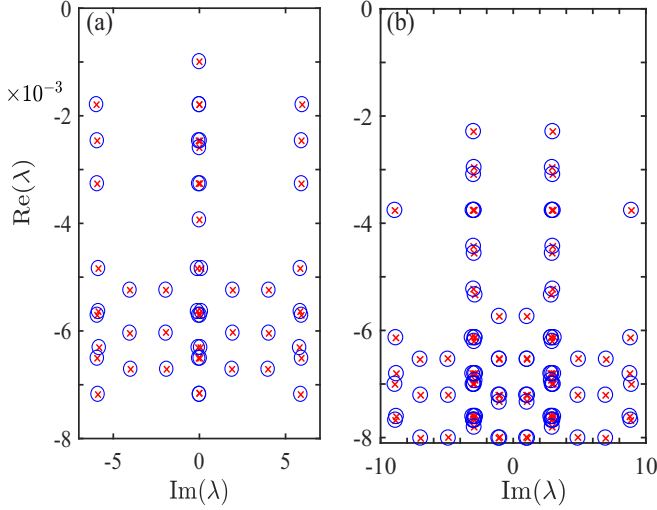


FIG. 3. Eigenvalues of the superoperator \mathcal{L} and multiple timescales in the subspaces \mathcal{K}_2 (a) and \mathcal{K}_3 (b) with $g_1 = 1, g_2 = 0.5, \gamma = 0.5$, and $N = 30$ (by open circles). For comparison, we also present $\lambda_i^1 + \lambda_j^1$ in (a) and $\lambda_i^1 + \lambda_j^1 + \lambda_k^1$ in (b) with crosses [see Eq. (20)], where λ_i^1 are eigenvalues of \mathcal{L} in the subspace \mathcal{K}_1 . The relative error is estimated to be of the order of 10^{-5} . Some of the lowest eigenvalues in the subspaces $\mathcal{K}_1, \mathcal{K}_2$, and \mathcal{K}_3 are listed in Table I.

and 2(f), the decay processes have the same oscillation period due to the finite coupling between the two edge modes, which in the many-body case will have the same energy splitting in the two ground-state energy in the XY model [see Fig. 1(a) and Eq. (8)]. However, in an odd chain, this oscillation will disappear due to the absence of coupling.

IV. EVOLUTION OF THE SINGLE-PARTICLE DENSITY MATRIX

A. Relaxation in the long-chain limit

The above results have established a connection of many-body dynamics and single-particle dynamics in the long-time limit for the dynamics of the ground state in the quantum XY model. From the symmetry point of view, the steady solution $\bar{\rho}$ has also been well understood. However, some more issues need to be explained. (1) Why $\text{Re}(\lambda_{2\sigma})$ exhibits an inflexion point at $\gamma_c \sim 1$; (2) What will happen in the long-chain limit? (3) What are the different roles played by the edge modes and bulk modes during relaxation? We focus on the subspace \mathcal{K}_1 , in which the dynamics of ψ_i is given by the following non-Hermitian Schrödinger equation [see Fig. 5(a)]:

$$i\partial_t \Psi = 2(H_0 + i\Gamma)\Psi, \quad (21)$$

where $\Gamma = \text{diag}(-\gamma, 0, \dots, 0, -\gamma)$ and

$$H_0 = \begin{pmatrix} 0 & ig_2 & 0 & \cdots & 0 \\ -ig_2 & 0 & ig_1 & \cdots & 0 \\ 0 & -ig_1 & 0 & \ddots & 0 \\ \vdots & \vdots & \ddots & \ddots & ig_2 \\ 0 & 0 & 0 & -ig_2 & 0 \end{pmatrix}. \quad (22)$$

TABLE I. Several eigenvalues in the subspaces $\mathcal{K}_1, \mathcal{K}_2$, and \mathcal{K}_3 for the results presented in Fig. 3 with $g_1 = 1, g_2 = 0.5, \gamma = 0.5$, and $N = 30$. In the last line, the relative error of $\lambda_{2,3}^k$ indicates the high accuracy of Eq. (20).

\mathcal{K}_1	λ_1^1	$-0.00050 - 2.98579i$	λ_1^1
	λ_2^1	$-0.00050 + 2.98579i$	λ_2^1
	λ_3^1	$-0.00130 - 2.98548i$	λ_3^1
	λ_4^1	$-0.00130 + 2.98548i$	λ_4^1
	λ_5^1	$-0.00197 - 2.94336i$	λ_5^1
	λ_6^1	$-0.00197 + 2.94336i$	λ_6^1
\mathcal{K}_2	λ_7^2	$-0.00010 + 0.00000i$	$\sim \lambda_1^1 + \lambda_2^1$
	λ_8^2	$-0.00180 - 0.00031i$	$\sim \lambda_1^1 + \lambda_4^1$
	λ_9^2	$-0.00180 + 0.00031i$	$\sim \lambda_2^1 + \lambda_3^1$
	λ_{10}^2	$-0.00180 - 5.97127i$	$\sim \lambda_1^1 + \lambda_3^1$
	λ_{11}^2	$-0.00180 + 5.97127i$	$\sim \lambda_2^1 + \lambda_4^1$
	λ_{12}^2	$-0.00247 - 0.04243i$	$\sim \lambda_1^1 + \lambda_6^1$
	λ_{13}^2	$-0.00247 + 0.04243i$	$\sim \lambda_2^1 + \lambda_5^1$
	λ_{14}^2	$-0.00247 - 5.92915i$	$\sim \lambda_1^1 + \lambda_5^1$
	λ_{15}^2	$-0.00247 + 5.92915i$	$\sim \lambda_2^1 + \lambda_6^1$
	λ_{16}^2	$-0.00259 + 0.00000i$	$\sim \lambda_3^1 + \lambda_4^1$
\mathcal{K}_3	λ_{17}^3	$-0.00229 - 2.98548i$	$\sim \lambda_1^1 + \lambda_2^1 + \lambda_3^1$
	λ_{18}^3	$-0.00229 + 2.98548i$	$\sim \lambda_1^1 + \lambda_2^1 + \lambda_4^1$
	λ_{19}^3	$-0.00296 - 2.94336i$	$\sim \lambda_1^1 + \lambda_2^1 + \lambda_5^1$
	λ_{20}^3	$-0.00296 + 2.94336i$	$\sim \lambda_1^1 + \lambda_2^1 + \lambda_6^1$
	λ_{21}^3	$-0.00309 - 2.98579i$	$\sim \lambda_1^1 + \lambda_3^1 + \lambda_4^1$
	λ_{22}^3	$-0.00309 + 2.98579i$	$\sim \lambda_2^1 + \lambda_3^1 + \lambda_4^1$
	λ_{23}^3	$-0.00376 - 2.94366i$	$\sim \lambda_1^1 + \lambda_4^1 + \lambda_5^1$
	λ_{24}^3	$-0.00376 + 2.94366i$	$\sim \lambda_2^1 + \lambda_3^1 + \lambda_6^1$
	λ_{25}^3	$-0.00376 - 8.91464i$	$\sim \lambda_1^1 + \lambda_3^1 + \lambda_5^1$
	λ_{26}^3	$-0.00376 + 8.91464i$	$\sim \lambda_2^1 + \lambda_4^1 + \lambda_6^1$
$\delta\lambda_i^k : \lambda_i^k - \sum_j \lambda_j^1 / \lambda_i^k \sim 10^{-5}$			

Here we have defined $\Psi = (\psi_1, \psi_4, \psi_5, \dots)$ in chain A, while its treatment for chain B is rather similar (see Appendix C). The eigenvalues in this bordered matrix are determined by [52–55]

$$\Delta_N = \frac{(g_1 g_2)^{m-1}}{\sin \theta} \left[g_1 g_2 (2i\gamma + \epsilon) \sin(m+1)\theta + (-\gamma^2 \epsilon + ig_1^2 \gamma + ig_2^2 \gamma) \sin(m\theta) \right] = 0, \quad (23)$$

when $N = 2m + 1$ is odd; and

$$\Delta_N = \frac{(g_1 g_2)^{m-1}}{\sin \theta} \left[(-\gamma^2 + g_1^2 + i2\gamma\epsilon) \sin(m\theta) + g_1 g_2 \sin(m+1)\theta - \gamma^2 \frac{g_2}{g_1} \sin(m-1)\theta \right] = 0, \quad (24)$$

when $N = 2m$ is even. In the above equations, ϵ is the eigenvalue and its relation to θ is determined by

$$\epsilon^2 = g_1^2 + g_2^2 + 2g_1 g_2 \cos \theta. \quad (25)$$

The above equations will be reduced to some well-known results in some limiting cases. In an odd chain, Eq. (23) will

be reduced to

$$\Delta_N = \frac{(g_1 g_2)^{m-1}}{\sin(\theta)} \sin[(m+1)\theta] = 0, \quad (26)$$

in which the solution is $\theta = \pi n/(m+1)$ for $n = 0, 1, 2, \dots, m$. In an even chain and long-chain limit, Eq. (24) will be reduced to

$$\Delta_N = \frac{(g_1 g_2)^{m-1}}{\sin(\theta)} [g_1^2 \sin(m\theta) + g_1 g_2 \sin((m+1)\theta)] = 0; \quad (27)$$

the solution is $\theta = n\pi/m - ng_2\pi/[(g_1 + g_2)m^2] + O(m^{-3})$.

We find that for the extended bands, the eigenvalues and the phases can be written as

$$\epsilon_n = \epsilon_{n,r} - i\epsilon_{n,i}, \quad \theta_n = \frac{n\pi}{m+1} + z_{n,r} + iz_{n,i}, \quad (28)$$

where $n \ll m$ and $\epsilon_{n,i}, z_{n,r}, z_{n,i}$ are small numbers in the sense that

$$\lim_{m \rightarrow \infty} m z_{n,i}/r = 0. \quad (29)$$

These solutions can be obtained by linearizing the above nonlinear equations (see details in Appendix D).

B. Solutions in some limiting conditions

(a) In the weak dissipation limit ($\gamma \ll g_1, g_2$) and in the odd (o) and even (e) chains, we have

$$\epsilon_{n,i}^o = \frac{(g_1^2 + g_2^2)n^2\pi^2\gamma}{(g_1 + g_2)^2m^3}, \quad \epsilon_{n,i}^e = \frac{2g_2^2n^2\pi^2\gamma}{(g_1 + g_2)^2m^3}. \quad (30)$$

One can easily check our previous approximation that $\lim_{m \rightarrow \infty} m z_{n,i}/r = 0$. The imaginary part of ϵ is responsible for the characteristic relaxation time T^* as

$$T^* = \max[1/(2\epsilon_{n,i})]. \quad (31)$$

This definition is consistent with that in Refs. [12,13], which is based on the inverse gap of the Liouvillian equation in the dissipative systems. This result accounts for the multiple timescales during relaxation, which should be a typical feature of many-body relaxation. When $\gamma \rightarrow 0$, $T^* \rightarrow \infty$, indicating of persistent coherent dynamics. Since $\epsilon_{n,i} \propto \gamma$, we have

$$T^* \propto \frac{N^3}{\gamma}, \quad (32)$$

which means that in the weak dissipation limit, relaxation is still important and can happen in a finite system. Moreover, we find that the odd-even effect is still visible in the long-chain limit.

(b) In the strong dissipation limit, the odd-even effect will vanish, and we find

$$\epsilon_{n,i} = \frac{2g_1^2g_2^2n^2\pi^2}{(g_1 + g_2)^2m^3\gamma}. \quad (33)$$

We are surprised to find that in the strong dissipation limit, the relaxation time

$$T^* \propto \gamma N^3, \quad (34)$$

thus it will be prolonged by the dissipation. The crossover between these two cases are determined by $\epsilon_{n,i} = \epsilon_{n,i}^i$ with $i = e, o$, which yields $\gamma_c = g_1$ in an even chain; and $\gamma_c = \sqrt{2}g_1g_2/\sqrt{g_1^2 + g_2^2}$ in an odd chain. Thus, the strong dissipation regime can be assigned by $\gamma > \gamma_c$. These inflexion

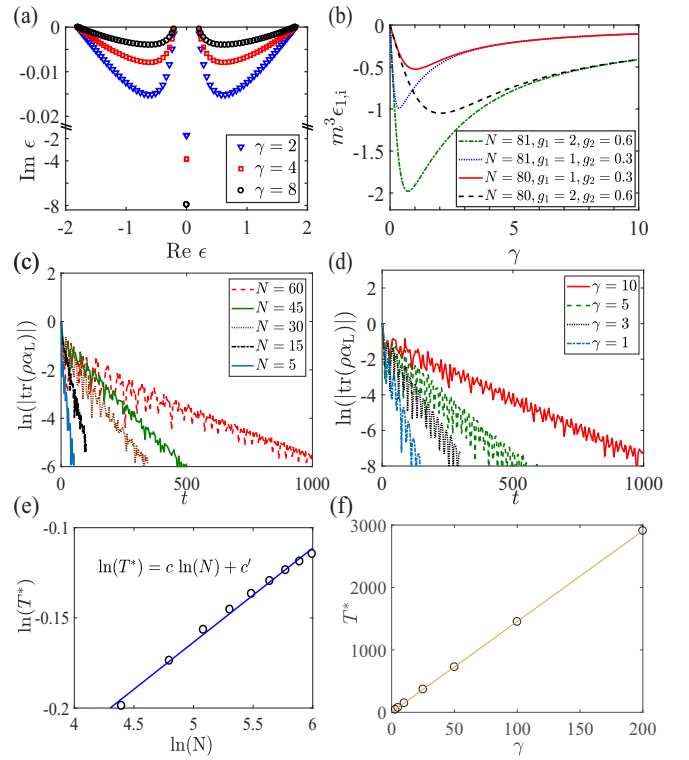


FIG. 4. (a) Spectra of the non-Hermitian matrix $H_0 + i\Gamma$ for $g_1 = 1$, $g_2 = 0.8$, $N = 80$ with different dissipation rates $\gamma = 2, 4, 8$. (b) $m^3 \epsilon_{1,i}$ as a function of γ and the odd-even effect with $N = 81$ and $N = 80$. (c) Long-time evolution of $\text{tr}(\rho \alpha_L)$ for different chains with parameters $g_1 = 1$, $g_2 = 0.9$, $\gamma = 10$. (d) Long-time evolution of $\text{tr}(\rho \alpha_L)$ for different dissipation rates with $g_1 = 1$, $g_2 = 0.95$, $N = 81$. (e) Scaling of $\ln T^* \sim c \ln N$ [see Eq. (47)], with fitted parameter $c = 2.3$ in this time window. (f) gives the scaling law of $T^* \propto \gamma$. In (c, d), $\rho(0)$ is the same as that used in Figs. 2(c) and 2(d).

points are also numerically verified, which are presented in Fig. 4(b). The above solutions are also approximately correct even in a short chain for the fast decay of the imaginary energy according to $\epsilon_{n,i} \propto 1/N^3$.

For the localized edge modes, a new decomposition is required. In the weak dissipation limit, the edge modes are not changed by the dissipation and we can make a perturbation around $\cos(\theta_c) = -(g_1^2 + g_2^2)/(2g_1g_2)$, which yields

$$\epsilon_L = \epsilon_R = -i\gamma(1 - \lambda^2), \quad (35)$$

for the two modes at the left and right ends. In the strong dissipation limit, the edge modes will be fully localized at the two open ends, thus we can assume $\epsilon \simeq -i\gamma$, and by perturbation about $\cos(\theta_c) = -(\gamma^2 + g_1^2 + g_2^2)/(2g_1g_2)$, we have

$$\epsilon_L = -i\gamma + ig_2^2/\gamma, \quad \epsilon_R = -i\gamma + ig_1^2/\gamma \quad (36)$$

in the odd chain and

$$\epsilon_L = \epsilon_R = -i\gamma + ig_2^2/\gamma \quad (37)$$

in the even chain. The details for these solutions can be found in Appendix D. These results are independent of chain length, indicating that in the long-chain limit the relaxation time is

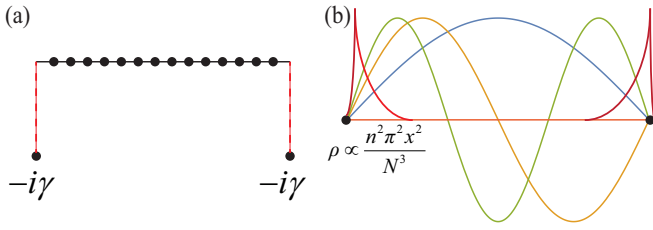


FIG. 5. Understanding of the relaxation process induced by boundary dissipation. (a) Effective Hamiltonian with boundary complex potential. (b) Single-particle wave functions and their overlaps with the edge dissipation. Here $N = 2m$ or $2m + 1$ is the total chain length (see text).

fully determined by the bulk bands, while the edge modes are most vulnerable to dissipation.

V. UNDERSTANDING OF THESE RESULTS USING PERTURBATION THEORY

The results in Eqs. (32) and (34) can be understood intuitively as follows. In the weak dissipation limit, the eigenstates are determined by the unperturbed Hamiltonian, where the dissipation can be introduced via the first-order perturbation process, which leads to decreasing of relaxation time with the increasing of dissipation. This is a common feature of all quantum qubits in the environment. However, in the strong dissipation limit, the boundary dissipation is so strong that it can no longer be treated as a perturbation. We expect that the wave functions at the two open ends are quickly dissipated, leaving the other bulk lattice sites unaffected. In this case, the larger the energy difference between the bulk bands and the two open ends is, the weaker their coupling will be, which leads to the decreasing of relaxation time with the increasing of dissipation rate. One should notice that in our model, we characterize the total relaxation time in terms of the mode(s) with the longest relaxation time [see Eq. (31)], thus the fast relaxation modes will not be important for T^* .

Based on the above picture, let us try to understand these anomalous results using perturbation theory (see Fig. 5). First, in the weak dissipation limit we can treat Γ as a perturbation. Based on the first-order perturbation theory, we find that for the localized edge modes, we have

$$\epsilon_L = \text{Im}\langle \psi_e | i\Gamma | \psi_e \rangle = -i\gamma |\psi_e(1)|^2 = -i\gamma(1 - \lambda^2), \quad (38)$$

with wave function at the left end as $\psi_e \sim (1, 0, \lambda, 0, \lambda^2, \dots)$ [see Fig. 5(b)]. In this case, the dissipation is independent of the total chain length. For the extended bands in an even chain and in the long-chain limit, the amplitude of the wave function at each site x is

$$\psi_e^n(x, \lambda) \propto \begin{cases} \sin\left(\frac{n\pi x}{N + \frac{2\lambda}{1+\lambda}}\right), & x \in e, \\ \sin\left(\frac{n\pi(N+1-x)}{N + \frac{2\lambda}{1+\lambda}}\right), & x \in o, \end{cases} \quad (39)$$

where n is the band index. In an odd chain,

$$\psi_o^n(x, \lambda) \propto \begin{cases} \sqrt{\lambda^2 + 1 + 2\lambda \cos \theta_n} \sin\left(\frac{(N-x+1)\theta_n}{2}\right), & x \in e, \\ \lambda \sin\left(\left(\frac{N-x}{2} + 1\right)\theta_n\right) + \sin\left(\frac{L-x}{2}\theta_n\right), & x \in o, \end{cases} \quad (40)$$

where $\theta_n = \frac{2n\pi}{N+1}$. These wave function need to be normalized. Then we find $\epsilon_{n,i} = \langle \psi_N^n | \Gamma | \psi_N^n \rangle$, which will recover the expression in Eq. (30).

In the strong dissipation limit, we need a different decomposition,

$$H_0 + i\Gamma = \mathcal{H}_0 + i\Gamma + V, \quad (41)$$

where we have used

$$\mathcal{H}_0 = \mathcal{P}_1 H_0 \mathcal{P}_1, \quad (42)$$

with \mathcal{P}_1 being the projector into the zero subspace of $i\Gamma$, that is $\mathcal{P}_1 = \text{diag}(0, 1, \dots, 1, 0)$. This decomposition follows exactly the mechanism presented at the beginning of this section for the reason that the dissipation sites decay much faster than the nondissipated regime.

After a few algebra, we find

$$V = \begin{pmatrix} 0 & ig_2 & 0 & \cdots & 0 \\ -ig_2 & 0 & 0 & \cdots & 0 \\ 0 & 0 & 0 & \ddots & 0 \\ \vdots & \vdots & \ddots & \ddots & ig_2 \\ 0 & 0 & 0 & -ig_2 & 0 \end{pmatrix}, \quad (43)$$

which contains only the coupling at sites 2 and $L - 1$, while all the other couplings are equal to zero exactly. \mathcal{H}_0 can be obtained by extracting V from H_0 [see Eq. (22)]. We can treat V as a perturbation, and via the second-order perturbation theory, we have

$$\epsilon_{n,i} \propto - \sum_{j=a,b} \frac{\langle \tilde{\psi}_N^n | V | j \rangle \langle j | V | \tilde{\psi}_N^n \rangle}{(E_n - E_j)}. \quad (44)$$

We first calculate the wave functions of the nonperturbative Hamiltonian $\mathcal{H}_0 + i\Gamma$, where the extended bands

$$\tilde{\psi}_N^n(x, \lambda) \propto \begin{cases} 0, & x = 1, N, \\ \psi_{N-2}^n(x-1, \lambda^{-1}), & x = 2, \dots, N-1, \end{cases} \quad (45)$$

and the localized modes

$$|a\rangle = (1, 0, 0, \dots), \quad |b\rangle = (\dots, 0, 0, 1). \quad (46)$$

This expression yields Eq. (33) [see the overlap between the bulk modes and the edge dissipation in Fig. 5(b)].

We present the dynamics of $\text{tr}(\rho \alpha_L)$ in Fig. 4(c), where α_L is the localized edge modes without dissipation. Since strong dissipation can influence the profile of the edge modes dramatically, α_L is no longer the eigenvector of $H_0 + i\Gamma$. By a linear fitting we find

$$\ln T^* = c \ln N + c', \quad (47)$$

where $c \sim 2.3$. The exponent of $c = 3$ is not reached due to the finite time window in simulation. This is because we only consider the dissipation of the extended bands $|\tilde{\psi}_N^n\rangle$ which have nonzero overlap with the edge modes ($\langle \psi_e | \tilde{\psi}_N^n \rangle \neq 0$), thus the dynamics of $\text{tr}(\rho \alpha_L)$ is dominated by the extended bands in the long-time limit. However, it will not influence the scaling of T^* with respect to γ [see Fig. 4(d)], since all the bulk bands have the same scaling law $T^* \propto \gamma$.

VI. CONCLUSION

Dissipation in the many-body system is a fundamental problem that up to date has not yet been well understood. We explore the dissipation-induced relaxation in a quantum XY model with boundary dissipation, in which the relaxation is characterized by a characteristic time T^* . In the short-time limit, the many-body dissipation is dominated; however, in the long-time limit, it is fully determined by the dynamics of single-particle physics, thus we characterize T^* using the lifetime of single-particle bands. We explore the roles played by the edge modes and the bulk bands in T^* , and their scaling laws with respect to chain length N and dissipation rate γ . An intuitive picture based on an equivalent non-Hermitian model is proposed, which show that the weak dissipation limit and strong dissipation limit will have totally different mechanisms for dissipation. An perturbation theory, which is in accord with this picture, is also provided, which yields analytical results in excellent agreement with the numerical results. These results may also suggest that the lowest two states protected by a finite gap width can not serve as quantum memory under dissipation, which is consistent with the conclusions in the previous literature [34,56–60]. Our results may have universal significance in the understanding the dissipation in the many-body state in the environment, in which its short-time dynamics is determined by the many-body dissipation, while its long-time dynamics is given by the few-body or even single-particle dissipation. We expect this conclusion can advance our understanding of many-body dissipation.

ACKNOWLEDGMENTS

This work is supported by the National Key Research and Development Program in China (Grants No. 2017YFA0304504 and No. 2017YFA0304103) and the National Natural Science Foundation of China (NSFC) with Grants No. 11974334 and No. 11774328. M.G. is also supported by the National Youth Thousand Talents Program and the USTC startup funding.

APPENDIX A: SYMMETRY TRANSFORMATIONS IN THE QUANTUM XY MODEL WITH BOUNDARY DISSIPATION

The Hamiltonian of a quantum XY model is shown in Eq. (2) in the main text, which mainly focuses on the region $g_1 > g_2 > 0$. The other regions could be transformed to this condition by some unitary transformations, as shown below. Let us define the unitary operator $U_n(S, \theta)$, which rotates the spin along the S direction, then we can construct some unitary operators along the three axes

$$T_z = \prod_{n:\text{odd}} U_n(S^z, \pi), \quad (\text{A1})$$

$$T_x = \prod_{n:\text{odd}} U_n(S^x, \pi), \quad (\text{A2})$$

$$T_y = \prod_{n:\text{odd}} U_n(S^y, \pi). \quad (\text{A3})$$

from U_n . We find that

$$T_z \sigma_i^x T_z^\dagger = (-1)^i \sigma_i^x, \quad T_z \sigma_i^y T_z^\dagger = (-1)^i \sigma_i^y. \quad (\text{A4})$$

Then the transformation $T_z H_{XY} T_z^\dagger$ interchanges $g_1 \rightarrow -g_1$, $g_2 \rightarrow -g_2$. Similarly, $T_x H_{XY} T_x^\dagger$ interchanges $g_1 \rightarrow g_1$, $g_2 \rightarrow -g_2$, and $T_y H_{XY} T_y^\dagger$ interchanges $g_1 \rightarrow -g_1$, $g_2 \rightarrow g_2$. However, we can construct a nitary operator

$$S = \prod_n U_n(S^z, \pi/4), \quad (\text{A5})$$

which leads to

$$S \sigma_i^x S^\dagger = -\sigma_i^y, \quad S \sigma_i^y S^\dagger = \sigma_i^x. \quad (\text{A6})$$

Then the transformation $S H_{XY} S^\dagger$ interchanges $g_1 \rightarrow g_2$, $g_2 \rightarrow g_1$. By combining all these unitary transformations, we can reach all the regions with $\pm g_1$ and $\pm g_2$ of the XY model, and the point $g_1 = \pm g_2$ corresponds to the self-dual points as the boundary between different phases [see the phase diagram in Fig. 1(b)]. Notice that the above transformations will leave the Lindblad term invariant since these transformations will at most introduce a minus sign to σ_j^z , thus will not influence the boundary dissipation terms and the related physics.

APPENDIX B: DENSITY MATRIX REPRESENTATION

We illustrate the exact equivalence between the Majorana fermion representation and Pauli matrix representation using one and two spins. This equivalence was used in Eqs. (14) and (15), both of which have 4^N terms. In the earlier literature, this equivalence has been used for the calculation of entanglement entropy in various exactly solvable spin models [49]. We show this equivalence explicitly by provide several transparent examples for it. For a single spin model, we can write the density matrix as follows:

$$\rho_1 = \frac{1}{2}(\mathbb{I} + c_x \sigma^x + c_y \sigma^y + c_z \sigma^z), \quad (\text{B1})$$

where the unity matrix \mathbb{I} ensures that $\text{Tr}(\rho_1) = 1$. With the Jordan-Wigner transformation,

$$\alpha_1 = \sigma^x, \quad \alpha_2 = \sigma^y, \quad -i\alpha_x \alpha_y = \sigma^z, \quad (\text{B2})$$

where α_1 and α_2 are Majorana fermion operators, this single-particle density matrix can be written in Majorana fermion representation as

$$\rho_1 = \frac{1}{2}(\mathbb{I} + c_x \alpha_1 + c_y \alpha_2 - i c_z \alpha_1 \alpha_2). \quad (\text{B3})$$

We see a one-to-one correspondence between these two representations.

Let us then consider a two spin model, which is slightly more complicated. The density matrix for double spins can be written as

$$\begin{aligned} \rho_2 = & \frac{1}{4}(\mathbb{I} + c_{x0} \sigma_1^x + c_{y0} \sigma_1^y + c_{z0} \sigma_1^z + c_{0x} \sigma_2^x + c_{0y} \sigma_2^y \\ & + c_{0z} \sigma_2^z + c_{xx} \sigma_1^x \sigma_2^x + c_{xy} \sigma_1^x \sigma_2^y + c_{xz} \sigma_1^x \sigma_2^z + c_{yx} \sigma_1^y \sigma_2^x \\ & + c_{yy} \sigma_1^y \sigma_2^y + c_{yz} \sigma_1^y \sigma_2^z + c_{zx} \sigma_1^z \sigma_2^x + c_{zx} \sigma_1^z \sigma_2^y + c_{zz} \sigma_1^z \sigma_2^z). \end{aligned} \quad (\text{B4})$$

In the Majorana fermion representation, we have

$$\alpha_1 = \sigma_1^x, \quad \alpha_2 = \sigma_1^y, \quad \alpha_3 = \sigma_1^z \sigma_2^x, \quad \alpha_4 = \sigma_1^z \sigma_2^y, \quad (\text{B5})$$

then

$$\begin{aligned} \rho_2 = & \frac{1}{4}(\mathbb{I} + c_{x0} \alpha_1 + c_{y0} \alpha_2 - c_{z0} i \alpha_1 \alpha_2 - c_{0x} i \alpha_1 \alpha_2 \alpha_3 \\ & - c_{0y} i \alpha_1 \alpha_2 \alpha_4 - c_{0z} i \alpha_3 \alpha_4 - c_{xx} i \alpha_2 \alpha_3 - c_{xy} i \alpha_2 \alpha_4 \end{aligned}$$

$$\begin{aligned}
& -c_{xz}i\alpha_1\alpha_3\alpha_4 + c_{yx}i\alpha_1\alpha_3 + c_{yy}i\alpha_1\alpha_4 - c_{yz}i\alpha_2\alpha_3\alpha_4 \\
& + c_{zx}\alpha_3 + c_{zy}\alpha_4 - c_{zz}\alpha_1\alpha_2\alpha_3\alpha_4.
\end{aligned} \quad (B6)$$

We see that in the Majorana fermion representation, the basis can always be written in the way of Eq. (15). During the basis interchange between these two representations, we even find that the coefficients of the basis in the density matrix are exactly the same, which may differ at most by a prefactor $\pm i$ or a sign ± 1 (or equivalently a phase $\pi n/2$ with $n \in \{0, 1, 2, 3\}$), thus their magnitudes are the same.

In the following, we present two concrete examples to illustrate the above equivalent representations. For $\rho_2 = |\uparrow\uparrow\rangle\langle\uparrow\uparrow| = \frac{1}{4}(\mathbb{I} + \sigma_1^z + \sigma_2^z + \sigma_1^z\sigma_2^z)$, we have

$$\rho_2 = \frac{1}{4}(\mathbb{I} - i\alpha_1\alpha_2 - i\alpha_3\alpha_4 - \alpha_1\alpha_2\alpha_3\alpha_4). \quad (B7)$$

And for $\rho_2 = |++\rangle\langle++| = \frac{1}{4}(\mathbb{I} + \sigma_1^x + \sigma_2^x + \sigma_1^x\sigma_2^x)$, where $|+\rangle = (|\uparrow\rangle + |\downarrow\rangle)/\sqrt{2}$, we have

$$\rho_2 = \frac{1}{4}(\mathbb{I} + \alpha_1 - i\alpha_2\alpha_3 - i\alpha_1\alpha_2\alpha_3). \quad (B8)$$

APPENDIX C: CONSERVATION OF MAJORANA NUMBER AND SINGLE-PARTICLE DYNAMICS

Since the density matrix can be represented by the Majorana fermions in the way of Eq. (15), which forms a complete basis for the density matrix. We can calculate the dynamics of the Lindblad equation using the same basis. To this end, let us define the observables as $\psi_i = \text{Tr}(\rho\alpha_i)$, $\psi_{ij} = \text{Tr}(\rho\alpha_i\alpha_j)$ and $\psi_{ijk} = \text{Tr}(\rho\alpha_i\alpha_j\alpha_k)$ [see Eq. (18) in the main text] with $i \neq j \neq k$. From the Lindblad equation, we have

$$\begin{aligned}
\frac{d}{dt} \text{Tr}(\rho\alpha_i) &= -i \text{Tr}(H\rho\alpha_i - \rho H\alpha_i) \\
& - \gamma [\text{Tr}(\rho\alpha_i) + \text{Tr}(\alpha_1\alpha_2\rho\alpha_1\alpha_2\alpha_i)] \\
& - \gamma [\text{Tr}(\rho\alpha_i) + \text{Tr}(\alpha_{2N-1}\alpha_{2N}\rho\alpha_{2N-1}\alpha_{2N}\alpha_i)].
\end{aligned} \quad (C1)$$

Using the properties of the trace operator, the above equation is simplified to

$$\begin{aligned}
\frac{d}{dt} \text{tr}(\rho\alpha_i) &= -i \text{Tr}(\rho[\alpha_i, H]) - \gamma \text{Tr}(\rho\alpha_i) \\
& - \gamma \text{tr}(\rho\alpha_1\alpha_2\alpha_i\alpha_1\alpha_2) - \gamma \text{tr}(\rho\alpha_i) \\
& - \gamma \text{tr}(\rho\alpha_{2N-1}\alpha_{2N}\alpha_i\alpha_{2N-1}\alpha_{2N}).
\end{aligned} \quad (C2)$$

This solution can be further simplified using the properties of the Majorana fermion operators, with $\{\alpha_i, \alpha_j\} = 2\delta_{ij}$. For example, for $N = 6$, the A and B subchains in Fig. 1 are described by

$$\frac{d}{dt} \Psi_A = \begin{pmatrix} -2\gamma & 2g_2 & 0 & 0 & 0 & 0 \\ -2g_2 & 0 & 2g_1 & 0 & 0 & 0 \\ 0 & -2g_1 & 0 & 2g_2 & 0 & 0 \\ 0 & 0 & -2g_2 & 0 & 2g_1 & 0 \\ 0 & 0 & 0 & -2g_1 & 0 & 2g_2 \\ 0 & 0 & 0 & 0 & -2g_2 & -2\gamma \end{pmatrix} \Psi_A, \quad (C3)$$

where $\Psi_A = (\psi_1, \psi_4, \psi_5, \psi_8, \psi_9, \psi_{12})^T$; and

$$\frac{d}{dt} \Psi_B = \begin{pmatrix} -2\gamma & 2g_1 & 0 & 0 & 0 & 0 \\ -2g_1 & 0 & 2g_2 & 0 & 0 & 0 \\ 0 & -2g_2 & 0 & 2g_1 & 0 & 0 \\ 0 & 0 & -2g_1 & 0 & 2g_2 & 0 \\ 0 & 0 & 0 & -2g_2 & 0 & 2g_1 \\ 0 & 0 & 0 & 0 & -2g_1 & -2\gamma \end{pmatrix} \Psi_B, \quad (C4)$$

where $\Psi_B = (\psi_2, \psi_3, \psi_6, \psi_7, \psi_{10}, \psi_{11})^T$.

The conservation of Majorana numbers during dynamics with this particular Lindblad dissipation can be deduced in the following way. Let us denote $\prod_{k=1}^n \alpha_{m_k}$ as the product of n different Majorana fermion operators. The dynamics of this operator is given by

$$\begin{aligned}
\frac{d}{dt} \text{Tr} \left(\rho \prod_{k=1}^n \alpha_{m_k} \right) &= -i \text{Tr} \left(\rho \left[\prod_{k=1}^n \alpha_{m_k}, H \right] \right) \\
& - 2\gamma \text{Tr} \left(\rho \prod_{k=1}^n \alpha_{m_k} \right) - \gamma \text{Tr} \left(\rho \alpha_1 \alpha_2 \prod_{k=1}^n \alpha_{m_k} \alpha_1 \alpha_2 \right) \\
& - \gamma \text{Tr} \left(\rho \alpha_{2N-1} \alpha_{2N} \prod_{k=1}^n \alpha_{m_k} \alpha_{2N-1} \alpha_{2N} \right).
\end{aligned} \quad (C5)$$

For the Hamiltonian in the quadratic of Majorana operators [48], one can prove that $[\prod_{k=1}^n \alpha_{m_k}, H]$ either equals to zero or conserves the number of Majorana operators. However, due to the anticommuting relation of Majorana fermion, $\alpha_1\alpha_2(\prod_{k=1}^n \alpha_{m_k})\alpha_1\alpha_2 = \pm \prod_{k=1}^n \alpha_{m_k}$, where the sign \pm depend on the particular form of $\prod_{k=1}^n \alpha_{m_k}$. The same is true for $\alpha_{2N-1}\alpha_{2N}\prod_{k=1}^n \alpha_{m_k}\alpha_{2N-1}\alpha_{2N}$. So the dynamics conserves the number of Majorana operators and the dynamics of the variables in Eq. (18) will be restricted to their own subspaces. Otherwise, the hierarchy equations need to be considered, which then can be solved numerically with some truncation [51]. Based on this feature, in Appendix D, some analytical expressions will be obtained for the dynamics in \mathcal{K}_1 subspace in several limits, which is in accord with the mechanisms discussed in Sec. V.

APPENDIX D: ANALYTICAL SOLUTIONS IN SOME LIMITS

1. Extended bands in the odd chain

For odd chain with $N = 2m + 1$, we can expand the non-linear Eqs. (24) and (26) around the points

$$\epsilon_n = \epsilon_{n,r} + i\epsilon_{n,i}, \quad \theta_n = \frac{n\pi}{m+1} + z_{n,r} + iz_{n,i}, \quad (D1)$$

where n is the band index, which satisfies $n \ll m$, and $\epsilon_{n,i}, z_{n,r}, z_{n,i}$ are small numbers in the sense that

$$\lim_{m \rightarrow \infty} m z_{n,i}/r = 0, \quad \lim_{m \rightarrow \infty} m \epsilon_{n,i}/r = 0. \quad (D2)$$

For brevity, we define new variable

$$A = g_1 g_2, \quad B = g_1^2 + g_2^2. \quad (\text{D3})$$

Then the nonlinear equations can be reduced to

$$A(2i\gamma + \epsilon_n) \sin(m+1)\theta_n + (iB\gamma - \gamma^2\epsilon) \sin m\theta_n = 0, \quad (\text{D4})$$

and

$$\epsilon_n^2 = B + 2A \cos \theta_n. \quad (\text{D5})$$

Substituting Eq. (D1) into Eq. (D5) and making a Taylor expansion of $z_{n,r}$ and $\epsilon_{n,i}$, assuming Eq. (D2), we have

$$(\epsilon_{n,r} + i\epsilon_{n,i})^2 = B + 2A \left[1 - \frac{1}{2} \left(\frac{n\pi}{m+1} + z_{n,r} + iz_{n,i} \right)^2 \right]. \quad (\text{D6})$$

From the above solution, the real part and imaginary part, respectively, yield

$$\epsilon_{n,r} \simeq \sqrt{B + 2A}, \quad \epsilon_{n,i} \simeq -\frac{An\pi z_{n,i}}{(m+1)\sqrt{B + 2A}}. \quad (\text{D7})$$

In the same way, using Eqs. (D1) and (D4), we have

$$\begin{aligned} & A(2i\gamma + \epsilon_{n,r} + i\epsilon_{n,i})[(m+1)z_{n,r} + (m+1)iz_{n,i}] \\ & + (iB\gamma - \gamma^2\epsilon_{n,r} - \gamma^2i\epsilon_{n,i}) \\ & \times \left[-\frac{n\pi}{m+1} + mz_{n,r} + miz_{n,i} \right] = 0. \end{aligned} \quad (\text{D8})$$

The real part of the above equation gives

$$\begin{aligned} & A\epsilon_{n,r}(m+1)z_{n,r} - 2Ar(m+1)z_{n,i} - \gamma^2 m\epsilon_{n,r}z_{n,r} \\ & + \gamma^2\epsilon_{n,r}\frac{n\pi}{m+1} - Brmz_{n,i} = 0, \end{aligned} \quad (\text{D9})$$

and the imaginary part gives

$$\begin{aligned} & 2A\gamma(m+1)z_{n,r} + A\epsilon_{n,r}(m+1)z_{n,i} - \gamma^2\epsilon_{n,r}mz_{n,i} \\ & + B\gamma(mz_{n,r} - \frac{n\pi}{m+1}) + \gamma^2\epsilon_{n,i}\frac{n\pi}{m+1} = 0. \end{aligned} \quad (\text{D10})$$

From Eqs. (D9) and (D10), we obtain

$$z_{n,r} = -\frac{\pi\gamma^2 n(g_1 g_2 - g_1^2 - g_2^2)}{g_1^2 g_2^2 m^2}, \quad (\text{D11})$$

$$z_{n,i} = \frac{(g_1^2 + g_2^2)\pi\gamma n}{g_1 g_2 (g_1 + g_2)m^2}, \quad (\text{D12})$$

$$\epsilon_{n,i} = -\frac{(g_1^2 + g_2^2)n^2\pi^2\gamma}{(g_1 + g_2)^2 m^3}. \quad (\text{D13})$$

With this solution, we can readily check the requirement of Eq. (D2). We find that

$$mz_{n,r}, mz_{n,i} \propto \frac{1}{m}, \quad m\epsilon_{n,i} \propto \frac{1}{m^2}, \quad (\text{D14})$$

thus the perturbation assumption is always hold.

The same procedure can be used to calculate the physics in the strong dissipation limit. We ignore the detailed calculation

here and only present our major results

$$z_{n,r} = \frac{\pi n}{m^2} - \frac{\pi g_1 g_2 n}{\gamma^2 m^2}, \quad (\text{D15})$$

$$z_{n,i} = \frac{2\pi g_1 g_2 n}{\gamma m^2 (g_1 + g_2)}, \quad (\text{D16})$$

$$\epsilon_{n,i} = -\frac{2g_1^2 g_2^2 n^2 \pi^2}{(g_1 + g_2)^2 m^3 \gamma}. \quad (\text{D17})$$

These results always satisfy Eq. (D14), which also validate our assumption.

2. Extended bands in the even chain

For $N = 2m$, we can expand the nonlinear Eqs. (24) and (25) around the points

$$\epsilon_n = \epsilon_{n,r} + i\epsilon_{n,i}, \quad \theta_n = \frac{n\pi}{m} + z_{n,r} + iz_{n,i}. \quad (\text{D18})$$

For brevity, we define new variable $C = g_1^2$. We substitute Eq. (D18) into the nonlinear Eqs. (24) and (25) and make a Taylor expansion of $z_{n,r}$ and $\epsilon_{n,i}$, assuming Eq. (D2), we obtain

$$\begin{aligned} & [\gamma^2 - C - 2i\gamma\epsilon_{n,r} + 2\gamma\epsilon_{n,i}](mz_{n,r} + imz_{n,i}) \\ & - A \left[\frac{n\pi}{m} + (m+1)z_{n,r} + i(m+1)z_{n,i} \right] \\ & + \gamma^2 \frac{A}{C} \left[-\frac{n\pi}{m} + (m-1)z_{n,r} + i(m-1)z_{n,i} \right] = 0, \end{aligned} \quad (\text{D19})$$

as well as

$$(\epsilon_{n,r} + i\epsilon_{n,i})^2 = B + 2A \cos \left(\frac{n\pi}{m} + z_{n,r} + iz_{n,i} \right). \quad (\text{D20})$$

From the above solution, the real part and imaginary part, respectively, yield

$$\epsilon_{n,r} \simeq \sqrt{B + 2A}, \quad \epsilon_{n,i} \simeq -\frac{An\pi z_{n,i}}{m\epsilon_{n,r}}. \quad (\text{D21})$$

In the same way, using Eq. (D19), the real part of the above equation gives

$$\begin{aligned} & (\gamma^2 - C + 2\gamma\epsilon_{n,i})mz_{n,r} + 2\gamma\epsilon_{n,r}mz_{n,i} \\ & - A \left[\frac{n\pi}{m} + (m+1)z_{n,r} \right] + \gamma^2 \frac{A}{C} \left[-\frac{n\pi}{m} + (m-1)z_{n,r} \right] = 0, \end{aligned} \quad (\text{D22})$$

and the imaginary part gives

$$\begin{aligned} & (\gamma^2 - C + 2\gamma\epsilon_{n,i})mz_{n,i} - 2\gamma\epsilon_{n,r}mz_{n,r} - A(m+1)z_{n,i} \\ & + \gamma^2 \frac{A}{C} (m-1)z_{n,i} = 0. \end{aligned} \quad (\text{D23})$$

Combining Eqs. (D21)–(D23), we can solve these linear equations in the weak dissipation limit and find

$$z_{n,r} = -\frac{g_2 n \pi (g_1^2 - 2\gamma^2)}{g_1^2 m^2 (g_1 + g_2)}, \quad (\text{D24})$$

$$z_{n,i} = \frac{2g_2 \pi \gamma n}{g_1 (g_1 + g_2)m^2}, \quad (\text{D25})$$

$$\epsilon_{n,i} = -\frac{2g_2^2 n^2 \pi^2 \gamma}{(g_1 + g_2)^2 m^3}. \quad (\text{D26})$$

While in the strong dissipation limit, we have

$$z_{n,r} = \frac{g_2(\gamma^2 - 2g_1^2)\pi k}{\gamma^2 m^2(g_1 + g_2)}, \quad (\text{D27})$$

$$z_{n,i} = \frac{2g_1 g_2 n \pi}{\gamma m^2(g_1 + g_2)}, \quad (\text{D28})$$

$$\epsilon_{n,i} = -\frac{2g_1^2 g_2^2 n^2 \pi^2}{(g_1 + g_2)^2 m^3 \gamma}. \quad (\text{D29})$$

These results are also in accord with Eq. (D14).

3. Edge modes with strong dissipation

In this subsection we derive the dissipation of edge mode in the strong dissipation using Taylor expansion method. For $\gamma \gg g_1, g_2$ in the odd chain, we assume

$$\epsilon = \epsilon_r - i\gamma - i\epsilon_i, \quad (\text{D30})$$

where ϵ_i is small number in the sense $\lim_{\gamma \rightarrow \infty} \epsilon_i = 0$. From numerical result, we find $\epsilon_r \sim 0$ with modest m , and we may reasonably set $\epsilon_r = 0$. We substitute Eq. (D30) into Eqs. (23) and (25) and obtain

$$g_1 g_2 (2i\gamma - i\gamma - i\epsilon_i) (\sin m\theta \cos \theta + \cos m\theta \sin \theta) + [\gamma^2 (i\gamma + i\epsilon_i) + i(g_1^2 + g_2^2)\gamma] \sin m\theta = 0 \quad (\text{D31})$$

and

$$\cos \theta = \frac{-(\gamma + \epsilon_i)^2 - g_1^2 - g_2^2}{2g_1 g_2}. \quad (\text{D32})$$

The above two solutions will yield $\sin \theta = -i\sqrt{(\frac{(\gamma + \epsilon_i)^2 + g_1^2 + g_2^2}{2g_1 g_2})^2 - 1}$, and $\lim_{m \rightarrow +\infty} \frac{\cos m\theta}{\sin m\theta} = -i$. Then Eq. (D31) can be written

$$(\gamma - \epsilon_i) \left[(\gamma + \epsilon_i)^2 + g_1^2 + g_2^2 - \frac{g_1^2 g_2^2}{\gamma^2} \right] - \gamma^2 (\gamma + \epsilon_i) - (g_1^2 + g_2^2)\gamma = 0. \quad (\text{D33})$$

By ignoring the higher-order terms of ϵ_i^3 , the above equation can be reduced to $\epsilon_i^2 \gamma + \epsilon_i (g_1^2 + g_2^2) + g_1^2 g_2^2 / \gamma = 0$, which yields

$$\epsilon_i = -\frac{g_1^2}{\gamma}, \quad \text{or} \quad \epsilon_i = -\frac{g_2^2}{\gamma}. \quad (\text{D34})$$

This solution is used in the main text in Eqs. (36) and (37).

For even chain, we substitute Eq. (D30) into Eq. (24) and obtain

$$[-\gamma^2 + g_1^2 + i2\gamma(-i\gamma - i\epsilon_i)] \sin m\theta + g_1 g_2 \sin(m+1)\theta - \gamma^2 \frac{g_2}{g_1} \sin(m-1)\theta = 0. \quad (\text{D35})$$

Using the properties of $\sin(\theta)$ and $\cos(\theta)$, we have

$$[\gamma^2 + g_2^2 + 2\gamma\epsilon_i][\cos \theta - i \sin \theta] + g_1 g_2 [(2 \cos^2 \theta - 1) - i2 \sin \theta \cos \theta] - \gamma^2 \frac{g_2}{g_1} = 0. \quad (\text{D36})$$

In the same way as the odd chain case, Eq. (D36) can be simplified as

$$\epsilon_i^2 + \frac{2\epsilon_i g_2^2}{\gamma} + \frac{g_2^4}{\gamma^2} = 0. \quad (\text{D37})$$

We have $\epsilon_i = -g_2^2/\gamma$, this result is used in Eq. (37) in the main text.

4. Edge modes with weak dissipation

In the weak dissipation limit, we can expand Eqs. (23), (24), and (25) around $\cos(\theta_c) = -(g_1^2 + g_2^2)/2g_1 g_2$. For the odd chain with $N = 2m + 1$, we assume

$$\theta = \theta_c + z_r + iz_i, \quad \epsilon = \epsilon_r + i\epsilon_i. \quad (\text{D38})$$

With the aid of numerical results, we find that ϵ_r and z_r decay exponentially to zero with the increasing of m , for which reason we can set $\epsilon_r = z_r = 0$ for large enough m . However, we find $\epsilon_i \propto \gamma$. We substitute Eq. (D38) into Eqs. (23) and (25) and make a Taylor expansion, obtaining

$$A(2\gamma + \epsilon_i)[-i \sin(m+1)\theta_c + \cos(m+1)\theta_c \cdot (m+1)z_i] + (-\gamma^2 \epsilon_i + B\gamma)(-i \sin m\theta_c + \cos m\theta_c \cdot mz_i) = 0 \quad (\text{D39})$$

and

$$\epsilon_i^2 = i2A \sin \theta_c z_i, \quad (\text{D40})$$

where θ_c satisfies

$$\cos \theta_c = -\frac{g_1^2 + g_2^2}{2g_1 g_2} = -\frac{B}{2A}, \quad \sin \theta_c = i\sqrt{\left(\frac{B}{2A}\right)^2 - 1}. \quad (\text{D41})$$

When m is large enough, we can prove

$$\lim_{\gamma \rightarrow 0} (m+1)z_i = 0, \quad \frac{\cos m\theta_c}{\sin m\theta_c} = i. \quad (\text{D42})$$

Then Eq. (D39) can be reduced to

$$A(2\gamma + \epsilon_i) \sin(m+1)\theta_c + B\gamma \sin m\theta_c = 0, \quad (\text{D43})$$

which leads to $\epsilon_i = -\gamma(1 - g_2^2/g_1^2)$.

For even chain $N = 2m$, We substitute Eq. (D38) into Eqs. (24) and (25) and have

$$(-\gamma^2 + g_1^2 - 2\gamma\epsilon_i)(\sin m\theta_c + \cos m\theta_c miz_i) + g_1 g_2 [\sin(m+1)\theta_c + \cos(m+1)\theta_c (m+1)iz_i] - \gamma^2 \frac{g_2}{g_1} [\sin(m-1)\theta_c + \cos(m-1)\theta_c (m-1)iz_i] = 0, \quad (\text{D44})$$

as well as Eq. (D40). With the aid of

$$\frac{\sin(m+1)\theta_c}{\sin m\theta_c} = -\frac{g_1}{g_2}, \quad \frac{\cos(m+1)\theta_c}{\sin m\theta_c} = -i\frac{g_1}{g_2}, \quad (\text{D45})$$

Eq. (D44) can be reduced to

$$-\gamma^2 - 2\gamma\epsilon_i + g_1^2 z_i + \gamma^2 \frac{g_2^2}{g_1^2} = 0, \quad (\text{D46})$$

which gives $\epsilon_i = -\gamma(1 - g_2^2/g_1^2)$. This solution has been used in Eq. (35) in the main text.

- [1] C. W. Gardiner and H. Haken, *Quantum Noise* (Springer, Berlin, 1991), Vol. 2.
- [2] J. R. Johansson, P. D. Nation, and F. Nori, Qutip: An open-source python framework for the dynamics of open quantum systems, *Comput. Phys. Commun.* **183**, 1760 (2012).
- [3] H. Weimer, Variational Principle for Steady States of Dissipative Quantum Many-Body Systems, *Phys. Rev. Lett.* **114**, 040402 (2015).
- [4] A. Le Boité, G. Orso, and C. Ciuti, Steady-State Phases and Tunneling-Induced Instabilities in the Driven Dissipative Bose-Hubbard Model, *Phys. Rev. Lett.* **110**, 233601 (2013).
- [5] D. Karevski, V. Popkov, and G. M. Schütz, Exact Matrix Product Solution for the Boundary-Driven Lindblad XXZ Chain, *Phys. Rev. Lett.* **110**, 047201 (2013).
- [6] T. Prosen, Exact Nonequilibrium Steady State of an Open Hubbard Chain, *Phys. Rev. Lett.* **112**, 030603 (2014).
- [7] T. Prosen, Exact Nonequilibrium Steady State of a Strongly Driven Open XXZ Chain, *Phys. Rev. Lett.* **107**, 137201 (2011).
- [8] D. A. Rowlands and A. Lamacraft, Noisy Spins and the Richardson-Gaudin Model, *Phys. Rev. Lett.* **120**, 090401 (2018).
- [9] L. Banchi, D. Burgarth, and M. J. Kastoryano, Driven Quantum Dynamics: Will It Blend? *Phys. Rev. X* **7**, 041015 (2017).
- [10] M. V. Medvedeva, F. H. L. Essler, and T. Prosen, Exact Bethe Ansatz Spectrum of a Tight-Binding Chain with Dephasing Noise, *Phys. Rev. Lett.* **117**, 137202 (2016).
- [11] P. Ribeiro and T. Prosen, Integrable Quantum Dynamics of Open Collective Spin Models, *Phys. Rev. Lett.* **122**, 010401 (2019).
- [12] Z. Cai and T. Barthel, Algebraic Versus Exponential Decoherence in Dissipative Many-Particle Systems, *Phys. Rev. Lett.* **111**, 150403 (2013).
- [13] M. Žnidarič, Relaxation times of dissipative many-body quantum systems, *Phys. Rev. E* **92**, 042143 (2015).
- [14] M. Žnidarič, Solvable quantum nonequilibrium model exhibiting a phase transition and a matrix product representation, *Phys. Rev. E* **83**, 011108 (2011).
- [15] M. Žnidarič, Exact solution for a diffusive nonequilibrium steady state of an open quantum chain, *J. Stat. Mech.* (2010) L05002.
- [16] In a many-body system, the dimension of the Hilbert $\text{Dim}(H)$ space increases exponentially with the size of the system. However, the dimension of the density matrix for the mixed space in open systems should be $\text{Dim}(H)^2$.
- [17] J. Eisert, M. Friesdorf, and C. Gogolin, Quantum many-body systems out of equilibrium, *Nat. Phys.* **11**, 124 (2015).
- [18] R. Nandkishore and D. A. Huse, Many-body localization and thermalization in quantum statistical mechanics, *Annu. Rev. Condens. Matter Phys.* **6**, 15 (2015).
- [19] H. Bernien, S. Schwartz, A. Keesling, H. Levine, A. Omran, H. Pichler, S. Choi, A. S. Zibrov, M. Endres, M. Greiner *et al.*, Probing many-body dynamics on a 51-atom quantum simulator, *Nature* **551**, 579 (2017).
- [20] C. J. Turner, A. A. Michailidis, D. A. Abanin, M. Serbyn, and Z. Papić, Weak ergodicity breaking from quantum many-body scars, *Nat. Phys.* **14**, 745 (2018).
- [21] C. J. Turner, A. A. Michailidis, D. A. Abanin, M. Serbyn, and Z. Papić, Quantum scarred eigenstates in a Rydberg atom chain: Entanglement, breakdown of thermalization, and stability to perturbations, *Phys. Rev. B* **98**, 155134 (2018).
- [22] C. Nayak, S. H. Simon, A. Stern, M. Freedman, and S. D. Sarma, Nonabelian anyons and topological quantum computation, *Rev. Mod. Phys.* **80**, 1083 (2008).
- [23] M. Freedman, A. Kitaev, M. Larsen, and Z. Wang, Topological quantum computation, *Bull. Amer. Math. Soc.* **40**, 31 (2003).
- [24] J. D. Sau, R. M. Lutchyn, S. Tewari, and S. D. Sarma, Generic New Platform for Topological Quantum Computation Using Semiconductor Heterostructures, *Phys. Rev. Lett.* **104**, 040502 (2010).
- [25] H. Zhang, C.-X. Liu, S. Gazibegovic, D. Xu, J. A. Logan, G. Wang, N. Van Loo, J. D. S. Bommer, M. W. A. De Moor, D. Car *et al.*, Quantized majorana conductance, *Nature* **556**, 74 (2018).
- [26] S. Nadj-Perge, I. K. Drozdov, J. Li, H. Chen, S. Jeon, J. Seo, A. H. MacDonald, B. A. Bernevig, and A. Yazdani, Observation of majorana fermions in ferromagnetic atomic chains on a superconductor, *Science* **346**, 602 (2014).
- [27] D. Wang, L. Kong, P. Fan, H. Chen, S. Zhu, W. Liu, L. Cao, Y. Sun, S. Du, J. Schneeloch *et al.*, Evidence for majorana bound states in an iron-based superconductor, *Science* **362**, 333 (2018).
- [28] H. H. Sun, K. W. Zhang, L. H. Hu, C. Li, G. Y. Wang, H. Y. Ma, Z. A. Xu, C. L. Gao, D. D. Guan, Y. Y. Li *et al.*, Majorana Zero Mode Detected with Spin Selective Andreev Reflection in the Vortex of a Topological Superconductor, *Phys. Rev. Lett.* **116**, 257003 (2016).
- [29] J. P. Xu, M. X. Wang, Z. L. Liu, J. F. Ge, X. Yang, C. Liu, Z. A. Xu, D. Guan, C. L. Gao, D. Qian *et al.*, Experimental Detection of a Majorana Mode in the Core of a Magnetic Vortex Inside a Topological Insulator-Superconductor $\text{Bi}_2\text{Te}_3/\text{NbSe}_2$ heterostructure, *Phys. Rev. Lett.* **114**, 017001 (2015).
- [30] Q. Liu, C. Chen, T. Zhang, R. Peng, Y. J. Yan, X. Lou, Y. L. Huang, J. P. Tian, X. L. Dong, G. W. Wang *et al.*, Robust and Clean Majorana Zero Mode in the Vortex Core of High-Temperature Superconductor $(\text{Li}_{0.84}\text{Fe}_{0.16})\text{OHFeSe}$, *Phys. Rev. X* **8**, 041056 (2018).
- [31] V. Mourik, K. Zuo, S. M. Frolov, S. R. Plissard, E. P. Bakkers, and L. P. Kouwenhoven, Signatures of majorana fermions in hybrid superconductor-semiconductor nanowire devices, *Science* **336**, 1003 (2012).
- [32] M. T. Deng, C. L. Yu, G. Y. Huang, M. Larsson, P. Caroff, and H. Q. Xu, Anomalous zero-bias conductance peak in a Nb-InSb Nanowire-Nb hybrid device, *Nano Lett.* **12**, 6414 (2012).
- [33] A. Das, Y. Ronen, Y. Most, Y. Oreg, M. Heiblum, and H. Shtrikman, Zero-bias peaks and splitting in an Al-InAs nanowire topological superconductor as a signature of majorana fermions, *Nat. Phys.* **8**, 887 (2012).
- [34] D. Rainis and D. Loss, Majorana qubit decoherence by quasi-particle poisoning, *Phys. Rev. B* **85**, 174533 (2012).
- [35] S. M. Albrecht, E. B. Hansen, A. P. Higginbotham, F. Kuemmeth, T. S. Jespersen, J. Nygård, P. Krogstrup, J. Danon, K. Flensberg, and C. M. Marcus, Transport Signatures of Quasi-particle Poisoning in a Majorana Island, *Phys. Rev. Lett.* **118**, 137701 (2017).
- [36] A. Y. Kitaev, Unpaired majorana fermions in quantum wires, *Phys. Usp.* **44**, 131 (2001).
- [37] A. Osterloh, L. Amico, G. Falci, and R. Fazio, Scaling of entanglement close to a quantum phase transition, *Nature* **416**, 608 (2002).

- [38] S. L. Zhu, Scaling of Geometric Phases Close to the Quantum Phase Transition in the XY Spin Chain, *Phys. Rev. Lett.* **96**, 077206 (2006).
- [39] J. Eisert and T. J. Osborne, General Entanglement Scaling Laws from Time Evolution, *Phys. Rev. Lett.* **97**, 150404 (2006).
- [40] T. J. Osborne and M. A. Nielsen, Entanglement in a simple quantum phase transition, *Phys. Rev. A* **66**, 032110 (2002).
- [41] J. M. Cheng, M. Gong, G. C. Guo, and Z. W. Zhou, Scaling of geometric phase and fidelity susceptibility across the critical points and their relations, *Phys. Rev. A* **95**, 062117 (2017).
- [42] M. Hein, W. Dür, and H.-J. Briegel, Entanglement properties of multipartite entangled states under the influence of decoherence, *Phys. Rev. A* **71**, 032350 (2005).
- [43] J. M. Cai, Z. W. Zhou, and G. C. Guo, Decoherence effects on the quantum spin channels, *Phys. Rev. A* **74**, 022328 (2006).
- [44] E. P. W. Pascual Jordan, About the Pauli exclusion principle, *Z. Phys.* **47**, 631 (1928).
- [45] S. Sachdev, *Quantum Phase Transitions* (Cambridge University Press, Cambridge, UK, 2011).
- [46] A. Kitaev and C. Laumann, Topological phases and quantum computation, [arXiv:0904.2771](https://arxiv.org/abs/0904.2771).
- [47] M. Cheng, R. M. Lutchyn, V. Galitski, and S. D. Sarma, Splitting of Majorana-Fermion Modes Due to Intervortex Tunneling in a $p_x + ip_y$ Superconductor, *Phys. Rev. Lett.* **103**, 107001 (2009).
- [48] T. Prosen, Third quantization: A general method to solve master equations for quadratic open fermi systems, *New J. Phys.* **10**, 043026 (2008).
- [49] G. Vidal, J. I. Latorre, E. Rico, and A. Kitaev, Entanglement in Quantum Critical Phenomena, *Phys. Rev. Lett.* **90**, 227902 (2003).
- [50] J. I. Latorre, E. Rico, and G. Vidal, Ground-state entanglement in quantum spin chains, *Quant. Inf. Comput.* **4**, 48 (2004).
- [51] R. J. Glauber, Time-dependent statistics of the Ising model, *J. Math. Phys.* **4**, 294 (1963).
- [52] L. Losonczi, Eigenvalues and eigenvectors of some tridiagonal matrices, *Acta Math. Hungarica* **60**, 309 (1992).
- [53] S. Kouachi, Eigenvalues and eigenvectors of tridiagonal matrices, *Electron. J. Linear Algebra* **15**, 8 (2006).
- [54] W. C. Yueh, Eigenvalues of several tridiagonal matrices, *Appl. Math. E-Notes* **5**, 66 (2005).
- [55] A. R. Willms, Analytic results for the eigenvalues of certain tridiagonal matrices, *SIAM J. Matrix Anal. Appl.* **30**, 639 (2008).
- [56] J. C. Budich, S. Walter, and B. Trauzettel, Failure of protection of majorana based qubits against decoherence, *Phys. Rev. B* **85**, 121405(R) (2012).
- [57] F. L. Pedrocchi and D. P. DiVincenzo, Majorana Braiding with Thermal Noise, *Phys. Rev. Lett.* **115**, 120402 (2015).
- [58] L. Mazza, M. Rizzi, M. D. Lukin, and J. I. Cirac, Robustness of quantum memories based on majorana zero modes, *Phys. Rev. B* **88**, 205142 (2013).
- [59] G. Goldstein and C. Chamon, Decay rates for topological memories encoded with majorana fermions, *Phys. Rev. B* **84**, 205109 (2011).
- [60] A. Carmele, M. Heyl, C. Kraus, and M. Dalmonte, Stretched exponential decay of majorana edge modes in many-body localized kitaev chains under dissipation, *Phys. Rev. B* **92**, 195107 (2015).